GEOPHYSICAL RESEARCH LETTERS, VOL. 35, L02207, doi:10.1029/2007GL032021, 2008

Distribution of the O_2 infrared nightglow observed with VIRTIS on board Venus Express

J.-C. Gérard,[1] A. Saglam,[1] G. Piccioni,[2] P. Drossart,[3] C. Cox,[1] S. Erard,[3] R. Hueso,[4] and A. Sánchez-Lavega[4]

Received 13 September 2007; revised 8 November 2007; accepted 21 November 2007; published 30 January 2008.

[1] We present characteristics of the statistical horizontal distribution of the O_2 infrared nightglow over most of the southern hemisphere observed with the VIRTIS instrument over a period spanning nearly 11 months of low solar activity. We show that the distribution is inhomogeneous with the regions of brightest emission reaching ~3 MegaRayleighs (MR) located at low latitude near and dawnward of the midnight meridian. The hemispherically averaged nadir brightness is 1.3 MR, in very good agreement with earlier ground based observations. We show that the dayside supply of O atoms is sufficient to produce the observed global O_2 nightglow if approximately 50% of the dayside O production is carried to the nightside by the subsolar to antisolar global circulation. Limb profiles observed at northern mid-latitudes exhibit large intensity variations over short time periods. Calculations with a one-dimensional chemical diffusive model produce an airglow peak at 96 km, in agreement with the limb observations. The atomic oxygen density derived from the best fits to O_2 airglow limb profiles reaches a maximum of $1.8-3.5 \times 10^{11}$ cm^{-3} at 104 km. **Citation:** Gérard, J.-C., A. Saglam, G. Piccioni, P. Drossart, C. Cox, S. Erard, R. Hueso, and A. Sánchez-Lavega (2008), Distribution of the O_2 infrared nightglow observed with VIRTIS on board Venus Express, *Geophys. Res. Lett.*, *35*, L02207, doi:10.1029/2007GL032021.

1. Introduction

[2] Molecular nightglow emissions from the upper lower thermosphere and upper mesosphere of Venus are a signature of the global thermospheric circulation in a region of the atmosphere which is hardly accessible to in situ measurements. Their brightness also provides an important tool to determine the density and distribution of constituents such as atomic oxygen and nitrogen. The morphology of the nitric oxide nightglow was analyzed by *Stewart et al.* [1980] based on measurements [*Bougher et al.*, 2006] made with the ultraviolet spectrometer on board Pioneer Venus. It is characterized by a large variability with a statistical maximum located 15° south of the equator and shifted by about 2 hours from midnight toward dawn. It was interpreted as evidence of a global thermospheric circulation from the day to the night side with a superimposed zonal superrotating component. The emission peak was found near 115 km [*Gérard et al.*, 1981]. The O_2 $^1\Delta_g \rightarrow {}^3\Sigma$ infrared airglow was first observed from the ground using a Fourier transform spectrometer by *Connes et al.* [1979]. It showed nearly equal brightness on both the day and the night sides. The nightside emission rate, corrected for reflection and emission angle, averaged over 6 nights was 1.2 ± 0.3 MegaRayleighs (MR). The O_2 $^1\Delta_g$ state appears to be formed by recombination of oxygen atoms produced on the dayside by photodissociation and electron impact dissociation of CO_2 and CO and transported to the nightside by the solar to antisolar (SSAS) circulation [*Bougher and Borucki*, 1994], where they recombine in three-body collisions:

$$O + O \rightarrow O_2^* + M \quad (1)$$

where O_2^* is one of the excited electronic states of the O_2 molecule. Further ground-based spatially resolved observations [*Allen et al.*, 1992; *Crisp et al.*, 1996; *Lellouch et al.*, 1997] showed that the spatial distribution is quite inhomogeneous, showing contrasts larger than 10 to 1 across the nightside. The emission rate was shown to locally exceed 5 MR with an hemispheric average of about 1.1 MR. The brightest regions are usually confined to 1000–2000 km diameter. These rapidly changing bright areas are observed at variable latitudes and local times, but most often located at low latitudes between midnight and 0300 local time. Rotational temperatures sometimes show correlations with the emission brightness, but the two quantities also exhibit independent variations [*Ohtsuki et al.*, 2005]. Based on early results from the Visible and InfraRed Thermal Imaging Spectrometer (VIRTIS) instrument on board the Venus Express orbiter, *Drossart et al.* [2007b] have presented nadir observations illustrating the highly structured nature of the oxygen airglow. The zonal apparent motions observed on the airglow are extremely variable from orbit to orbit although they are generally related to the visual aspect of the structures and will be presented elsewhere. The mean zonal apparent motion is 20 m s^{-1} (dawnward) and the mean meridional apparent motion is 10 m s^{-1} from the pole to the equator. VIRTIS images obtained every 30 min. show the variability is of short term with most of the details changing from one image to another but with the large structures usually surviving at least through 1–2 hours. However, individual VIRTIS images are spatially limited and do not provide a global view of the airglow morphology. Consequently, it is difficult from ground-based or from individual VIRTIS snapshot images

[1] Laboratoire de Physique Atmosphérique et Planétaire, Université de Liège, Liege, Belgium.
[2] Istituto Nazionale di Astrofisica and Istituto di Astrofisica Spaziale e Fisica Cosmica, Rome, Italy.
[3] Laboratoire d'Etudes Spatiales et d'Instrumentation en Astrophysique, Observatoire de Paris, CNRS, UPMC, Université Paris-Diderot, Meudon, France.
[4] Escuela Superior Ingeniería, Universidad del País Vasco, Bilbao, Spain.

0094-8276/08/2007GL032021$05.00

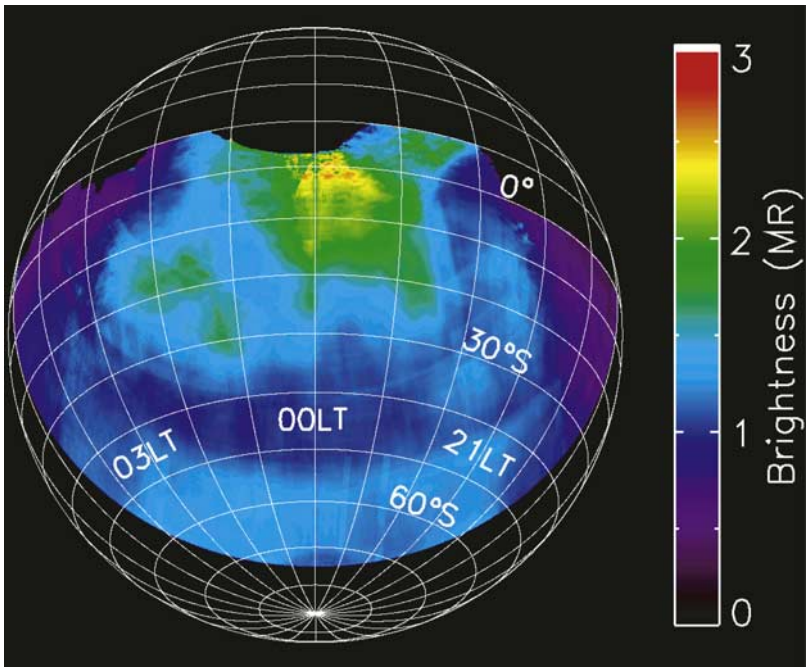

Figure 1. Global map of the vertical brightness (in MR) of the O_2 infrared nightglow observed with VIRTIS at low solar activity. The emission rate accounts for the component reflected by the clouds and the emission angle. The perspective is from 30° in the midnight meridian. Parallels are indicated every 10° and local time meridians are separated by 1 hour.

to build a statistical picture of the airglow morphology and relate it to the global thermospheric circulation.

[3] In this study, we characterize the statistical horizontal distribution of the O_2 infrared airglow over most of the southern hemisphere using a large set of VIRTIS images and we describe its vertical structure. We also address the question of the adequacy of the dayside supply of O atoms to produce the observed global O_2 nightglow. Finally, we compare observed limb profiles with the distribution calculated with a one-dimensional chemical diffusive model.

2. Morphology of the O_2 ($^1\Delta_g$) Nightglow

[4] The Venus Express orbit is elliptical with a period of 24 hours, an apocenter at 60,000 km and a pericenter at 250 km, located at 80°N. It is fixed in the inertial space so that it precesses in local time by 6.4 min/24 h. Spectral images have been regularly obtained in nadir geometry with VIRTIS mostly from segments of the orbit near apocenter. The VIRTIS [*Drossart et al.*, 2007a] pixel size of 0.25 mrad gives a spatial resolution of 15 km on Venus from apocenter. For this study, we use the VIRTIS M-mode which provides spectral cubes between 0.25 and 5 mm at a spectral resolution R ~200. Each spectral channel is ~9.5 nm wide in the region of the O_2 IR emission. A spatial scan, covering a 64 mrad × 64 mrad field of view, is generally obtained in about 10 minutes using a scanning mirror. In this study, we only include images collected from above 20000 km, but even from apocenter only a fraction of the Venus disk is observed during a mirror scan of the instrument and a spacecraft re-pointing is needed to have a more extended coverage.

[5] A total of 1225 images have been assembled to build a statistical view of the O_2 infrared emission, spanning a period extending from May 16, 2006 to April 7, 2007. The F10.7 daily solar activity index averaged over the days when observations were collected was low (74×10^{-22} W/m^2 Hz). For each image, the thermal contribution from the lower atmosphere is subtracted from the total signal using the VIRTIS fluxes measured in the three adjacent channels centred on 1.27 μm, the thermal distributions measured by *Crisp et al.* [1996] and the theoretical O_2 ($^1\Delta_g$) relative line intensity for a temperature of 200 K. The resulting 1.27 μm flux image is then binned into 0.2° × 0.2° latitude-longitude cells. To account for airglow radiation emitted downward and subsequently backscattered by the underlying clouds and determine the primary emission rate, we use the correction factor derived by *Crisp et al.* [1996]. To account for the different emission angles, the intensity of each pixel is corrected by a Chapman factor. Once the brightness of all pixels in each image has been converted into a simulated vertical brightness, a global map is constructed by summing the contribution in each latitude-longitude bin and normalizing by the number of contributions to each spatial bin.

[6] Figure 1 shows the spherical projection of the average distribution of the 1.27 μm vertical brightness converted into MegaRayleigh units. The vantage point is located at midnight local time and a latitude of 30°S. We note that the northern hemisphere is essentially not covered, as a result of the Venus Express orbital configuration. The number of entries to each spatial bin varies from 447 at high southern latitudes to a few units near the equator. The distribution of O_2 ($^1\Delta$) intensity is characterized by a bright spot extending down to ~30°S along the midnight meridian with the highest emission rates (~2.5 MR) concentrated near the equator. A secondary bright region is centred near 20°S and 0140 local time. Other mid-latitude regions, especially those located more than 2.5 LT hours from local midnight are

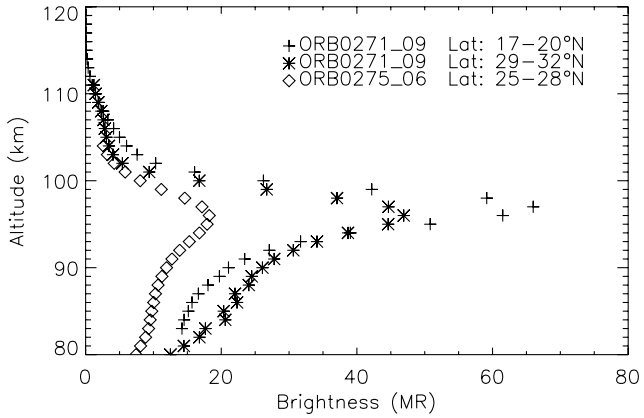

Figure 2. Limb profiles observed by VIRTIS on Venus Express orbits 271 and 275 at different northern latitudes.

dimmer. The average vertical emission rate is 1.3 MR, with a 1-σ variability of 0.7 MR. The darkest regions are at the ~0.3 MR level, giving a contrast ratio of about 10 between bright and dark regions. In contrast to the NO airglow, the brightest O_2 emission region is not shifted toward post-midnight. Instead, the highest O_2 intensities remain confined close to the midnight meridian, suggesting that the distribution of O atoms is more symmetrical at the altitude of the O_2 airglow layer than at the higher altitude of the NO emission. However the secondary O_2 bright region is shifted in the same direction as the nitric oxide maximum observed with Pioneer Venus. The higher level of symmetry observed here is consistent with the estimation of weaker mean zonal winds near 90–110 km (O_2 airglow layer) than in the 115–150 km region (NO airglow layer) as indicated by *Bougher et al.* [2006, Table 1] describing three-dimensional simulations.

[7] Figure 2 illustrates two limb profiles at 1.27 μm observed on orbit 271 (Jan. 16, 2007) averaged between 17°–20° and between 29°–32°N. In spite of the small distance separating the two profiles, a brightness difference exceeding 30% is observed, although the peak altitude remains close to 96 km in both cases. To further illustrate the variability, the limb profile at 25°–28°N from orbit 275 (Jan. 20, 2007) is also shown in Figure 2. Its peak reaches 18 MR at 96 km, but its brightness is significantly less than the profiles observed at similar latitudes four days earlier. These values compare favorably with the limb profile obtained on orbit 76 (July 5, 2006) by *Drossart et al.* [2007b] where the emission peak reached 33 MR at 96 km. Assuming spherical symmetry, the limb brightness is easily converted into vertical emission rate. They correspond to 0.3 MR, 0.61 MR and 0.63 MR respectively, that is close to the lower values observed on the south global map outside the two bright regions. The implications of these results on the flux of O atoms and the strength of the vertical transport are discussed below.

3. Photochemical-Diffusive Model

[8] To relate the average map of O_2 $^1\Delta_g$ to the downward flux of O atoms and analyze the airglow altitude distribution, we have developed a simple one-dimensional chemical-transport model. Reaction (1) has been identified as the source of $^1\Delta_g$ molecules. Other processes such as catalytic cycles involving OH or Cl have been proposed as possible additional sources of the $^1\Delta_g$ state, but the yield ε of $^1\Delta_g$ appears to be very small and the candidates have proven inadequate [*Leu and Yung*, 1987]. When O atoms recombine, only 7–8% the O_2 molecules are formed directly in the $^1\Delta_g$ state [*Bates*, 1988; *Wayne*, 1994]. However, it is estimated that the net production of this state may be considerably larger, as a result of the cascades from upper lying states into the $^1\Delta_g$ [*Krasnopolsky*, 1986]. We adopt an efficiency value $\varepsilon = 0.75$ as suggested by *Crisp et al.* [1996] Quenching of the O_2 $^1\Delta_g$ state whose radiative lifetime is ~4300 s [*Miller et al.*, 2001] occurs mostly by collisions with CO_2, causing non-radiative transitions to the O_2 ground state. Calculations based on a quenching coefficient by CO_2 of 2×10^{-20} cm^3 s^{-1} indicate that the collisional and the radiative lifetimes are equal at 91 km. At emission peak, approximately 80 % of the O_2 $^1\Delta_g$ molecules deactivate by emitting 1.27 μm photons. Consequently, the bottom of the airglow layer may drop faster with depth than the production rate of O_2 $^1\Delta_g$ molecules. Radiative recombination of O and N:

$$O + N \rightarrow NO \quad (2)$$

is the source of the NO nightglow, which has been observed on Earth, Venus and Mars but is of secondary importance as a loss of atomic oxygen on the nightside. The model solves the one-dimensional continuity equations:

$$\partial n_i/\partial t = P_i - L_i - \partial \Phi_i/\partial z \quad (3)$$

for n_i = O(^{3}P), N(^{4}S), NO, O_2 and O_2 ($^1\Delta_g$) using a finite volume method, with P_i and L_i the chemical production and loss rates respectively and Φ_i the vertical flux of the i_{th} component. The rate coefficients are adopted from *Slanger et al.* [2006]. The upper and lower boundaries are set at 130 and 80 km, respectively. A downward flux of O atoms flows through the upper boundary under the effect of molecular and eddy diffusion. The constituents are assumed to be in photochemical equilibrium at the lower boundary. As the O atoms move downward, they are progressively consumed by reactions (1) and (2). The temperature and CO_2 vertical distributions are taken from the semi-empirical model by *Hedin et al.* [1983], based on Pioneer Venus in situ measurements extended below 140 km with the VIRA model. In this one-dimensional representation, vertical transport at high altitude is ensured by molecular diffusion. Below the homopause, transport is parameterized by an eddy diffusion coefficient in the form $K = A/\sqrt{n}$ cm^2 s^{-1}, where A is an empirically estimated parameter and n is the number density in cm^{-3}. The altitude of the peak of the 1.27-μm emission is mainly controlled by eddy mixing, while the brightness responds to the downward flux of O atoms crossing the upper boundary. Using ε = 0.75 and noting that the loss of O atoms by reaction 2 in a vertical column is about four orders of magnitude less than by reaction (1), we obtain the relationship $I_{nadir} = 0.37 \times 10^{-12}$ Φ_O between the vertical emission rate I_{nadir} (in MR) and the downward flux Φ_O (in cm^{-2} s^{-1}) at 130 km. Consequently, the observed mean value of 1.3 MR corresponds to an average downward flux $\Phi_0 = 3.5 \times 10^{12}$ cm^{-2} s^{-1} in the

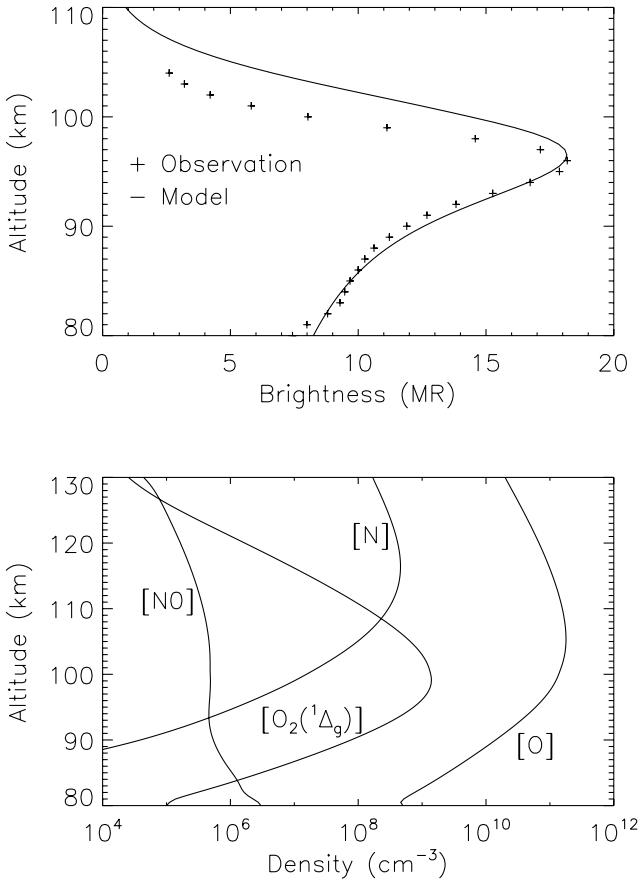

Figure 3. (top) Comparison between the O_2 airglow limb profile from orbit 275 at 25°–28°N and the calculated profile from the one-dimensional chemical-diffusive model. (bottom) Calculated vertical distribution of O, N(^{4}S), NO and O_2 ($^1\Delta_g$) densities for the same conditions as in Figure 3 (top).

southern hemisphere. This mean value may be compared with the average production on the dayside estimated to 8×10^{12} O atoms cm^{-2} s^{-1} [*Leu and Yung*, 1987]. It indicates that approximately half of the dayside production of O atoms is transported to the nightside where they recombine and produce the O_2 IR airglow.

[9] The best fit to the profile measured from orbit 275 at 26°N is shown in Figure 3 (top). It corresponds to a value of $A = 4 \times 10^{12}$, somewhat less than earlier determinations of 8×10^{12} to 2×10^{13} [*von Zahn et al.*, 1980; *Gérard et al.*, 1981] and a downward flux $F_0 = 3.8 \times 10^{11}$ cm^{-2} s^{-1}. This value is less than the average flux discussed in the previous paragraph, reflecting the relatively weak intensity of this particular limb profile. Although the peak altitude and the distribution below the maximum limb profile of the O_2 ($^1\Delta_g$) is reasonably well matched by the model, the airglow layer appears somewhat narrower than calculated. This difference suggests that the CO_2 density and/or temperature distributions or the parameterization of vertical transport adopted here may be partly inadequate. For example, vertical downward winds may play a role in redistributing oxygen atoms. Figure 3 (bottom) shows the altitude distribution of the O, N, NO and O_2 ($^1\Delta_g$) densities calculated with the downward O flux mentioned before and a downward N flux 1% of this value. The O peak density is 1.8×10^{11} cm^{-3} at 104 km, while the N maximum at 117 km is 4.6×10^8 cm^{-3}. The O maximum is 3×10^{11} cm^{-3} and 3.5×10^{11} cm^{-3} for the other two profiles of Figure 3 (top). These O density maxima are comparable to VIRA [*Keating et al.*, 1985] and *Massie et al.* [1983] who gave peak values of 2.6×10^{11} and 2.4×10^{11} cm^{-3}, respectively. They are also close to the O peak density of $\sim 3-4 \times 10^{11}$ cm^{-3} at 104 km which was simulated using the VTGCM with enhanced eddy diffusion [*Bougher and Borucki*, 1994].

4. Discussion

[10] We first note that the global morphology shown in Figure 1 is similar to many of the individual observations with a stream of nightglow close to midnight and another stream displaced about 2 hours in terms of local time. Observations of these streams indicate they usually evolve moving dawnward. Blobs of bright emission are sometimes superimposed with strong intensity variations in time-scales of 1 hour. As mentioned before, if symmetry is assumed between the hemispheres, the mean vertical intensity of 1.3 MR implies that nearly 50% of the dayside O atoms are transported to the nightside by the subsolar to antisolar global circulation. A transport efficiency of about 50% for the transfer of atomic oxygen from the day to the night side is in good agreement with the results of the three-dimensional model calculation by *Bougher and Borucki* [1994] who showed that the diurnal contrast of the O_2 airglow predicted by their model would be small if the peak is located near 98 km. However, the lower boundary of their 3-D model was too close (90 km) to the now measured altitude of the airglow layer to permit an accurate determination of the altitude of the emission maximum. Therefore, the 3-D model predicted an airglow peak at altitude between 103 and 107 km. It is likely that the adoption of a lower altitude boundary, a higher O_2 ($^1\Delta_g$) production efficiency and possibly a larger nightside eddy diffusion coefficient would result in a better agreement with these observations [*Bougher et al.*, 2006]. Future detailed observations will be necessary to investigate the similarities between the NO and the airglow distributions, in particular the identical location of the NO bright spot and the secondary bright O_2 $^1\Delta$ region observed in Figure 1. Finally, we note that the observed global average temperature of 186 K determined from the O_2 ($^1\Delta_g$) rotational distribution relates to typical altitudes of 96 ± 1 km. The nightside temperatures at 96 km of 169 K given by VIRA and 161 K by *Hedin et al.* [1983] are thus about 20 K less than those deduced from the airglow. A similar discrepancy was recently found from stellar occultation observations with the SPICAV spectrograph by *Bertaux et al.* [2007] who argue that the upper mesosphere-lower thermosphere nightside is warmer than previously expected.

[11] **Acknowledgments.** We gratefully thank all members of the ESA Venus Express project and of the VIRTIS scientific and technical teams (http://servirtis.obspm.fr/Venus_Express/VIRTIS_Team.html). J.C.G. acknowledges funding from the Belgian Fund for Scientific Research (FNRS). A. Saglam and C. Cox are supported the PRODEX program managed the European Space Agency with the help of the Belgian Federal Space Science Policy Office. RH and ASL acknowledge support from MEC AYA2003-03216 and Grupos UPV 15946/2004. This work is supported by the Centre National d'Etudes Spatiales and Agenzia Spaziale Italiana.

References

Allen, D., D. Crisp, and V. Meadows (1992), Variable oxygen airglow on Venus as a probe of atmospheric dynamics, *Nature*, *359*, 516.

Bates, D. R. (1988), Excitation and quenching of the oxygen bands in the nightglow, *Planet. Space Sci.*, *36*, 875.

Bertaux, J.-L., et al. (2007), A warm layer in Venus' cryosphere and high-altitude measurements of HF, HCl, H_2O and HDO, *Nature*, *450*, 549–646, doi:10.1038/nature05974.

Bougher, S. W., and W. J. Borucki (1994), Venus O_2 visible and IR nightglow: Implications for lower thermosphere dynamics and chemistry, *J. Geophys. Res.*, *99*, 3759.

Bougher, S. W., S. Rafkin, and P. Drossart (2006), Dynamics of the Venus upper atmosphere: Outstanding problems and new constraints expected from Venus Express, *Planet. Space Sci.*, *54*, 1371.

Connes, P., J. F. Noxon, W. A. Traub, and N. P. Carleton (1979), O_2 ($^1\Delta$) emission in the day and night airglow of Venus, *Astrophys. J.*, *233*, L29.

Crisp, D., V. S. Meadows, B. Bézard, C. de Bergh, J.-P. Maillard, and F. P. Mills (1996), Ground-based near-infrared observations of the Venus nightside: 1.27-μm O_2 (a $^1\Delta$g) airglow from the upper atmosphere, *J. Geophys. Res.*, *101*, 4577.

Drossart, P., et al. (2007a), Scientific goals for the observation of Venus by VIRTIS on ESA/Venus Express mission, *Planet. Space*, 55, 1653, doi:10.1016/j.pss.2007.01.003.

Drossart, P., et al. (2007b), A dynamic upper atmosphere of Venus as revealed by VIRTIS on Venus Express, *Nature*, *450*, 641–645, doi:10.1038/nature06140.

Gérard, J.-C., A. I. F. Stewart, and S. W. Bougher (1981), The altitude distribution of the Venus nightglow and implications on vertical transport, *Geophys. Res. Lett.*, *8*, 633.

Hedin, A. E., H. B. Niemann, W. T. Kasprzak, and A. Seiff (1983), Global empirical model of the Venus thermosphere, *J. Geophys. Res.*, *88*, 73.

Keating, G. M., et al. (1985), Venus international reference atmosphere, *Adv. Space Res.*, *5*, 117.

Krasnopolsky, V. A. (1986), Oxygen emissions in the night airglow of the Earth, Venus, and Mars, *Planet. Space Sci.*, *34*, 511.

Lellouch, E., T. Clancy, D. Crisp, A. Kliore, D. Titov, and S. W. Bougher (1997), Monitoring of mesospheric structure and dynamics, in *Venus*, vol. 2, *Geology, Geophysics, Atmosphere, and Solar Wind Environment*, edited by S. W. Bougher, D. M. Hunten, and R. J. Philips, pp. 295–324, Univ. of Ariz. Press, Tucson.

Leu, M. T., and Y. L. Yung (1987), Determination of the O_2 ($^1\Delta$) and O_2 ($^1\Sigma$) yields in the reaction O + ClO = Cl + O_2: Implications for photochemistry in the atmosphere of Venus, *Geophys. Res. Lett.*, *14*, 949.

Massie, S. T., D. M. Hunter, and D. T. Sowell (1983), Day and night models of the Venus thermosphere, *J. Geophys. Res.*, *88*, 3955.

Miller, H. C., J. E. McCord, J. Choy, and G. D. Hager (2001), Measurement of the radiative lifetime of O_2 ($a^1\Delta$g) using cavity ring down spectroscopy, *J. Quant. Spectrosc. Radiat. Transfer*, *69*, 305, doi:10.1016/S0022-4073 (00)00086-8.

Ohtsuki, S., N. Iwagami, H. Sagawa, H. Kasaba, Y. Ueno, and M. Imamura (2005), Groundbased observation of the Venus 1.27-μm O_2 airglow, *Adv. Space*, *36*, 2038.

Slanger, T., D. L. Huestis, P. C. Cosby, N. J. Chanover, and T. A. Bida (2006), The Venus nightglow ground-based observations and chemical mechanisms, *Icarus*, *182*, 1.

Stewart, A. I. F., J. C. Gérard, D. W. Rusch, and S. W. Bougher (1980), Morphology of the Venus ultraviolet night airglow, *J. Geophys. Res.*, *85*, 7861.

von Zahn, U., K. H. Fricke, D. M. Hunten, D. Krankowsky, K. Mauersberger, and A. O. Nier (1980), The upper atmosphere of Venus during morning conditions, *J. Geophys. Res.*, *85*, 7829.

Wayne, R. P. (1994), Singlet oxygen in the environmental sciences, *Res. Chem. Intermed.*, *20*, 395.

C. Cox, J.-C. Gérard, and A. Saglam, Laboratoire de Physique Atmosphérique et Planétaire, Université de Liège, allée du 6 août, B-4000 Liège, Belgium. (jc.gerard@ulg.ac.be)

P. Drossart and S. Erard, Laboratoire d'Etudes Spatiales et d'Instrumentation en Astrophysique, Observatoire de Paris, CNRS, UPMC, Université Paris-Diderot, 5 place Jules Janssen, F-92195 Meudon, France.

R. Hueso and A. Sánchez-Lavega, Escuela Superior Ingeniería, Universidad del País Vasco, Alameda Urquijo s/n, E-48013 Bilbao, Spain.

G. Piccioni, Istituto Nazionale di Astrofisica and Istituto di Astrofisica Spaziale e Fisica Cosmica, I-00133 Rome, Italy.